Scripta Materialia 133 (2017) 54–58

Contents lists available at ScienceDirect

Scripta Materialia

journal homepage: www.elsevier.com/locate/scriptamat

Regular Article

Mechanical properties of individual nanorods and nanotubes in forest-like structures

Jieun Park [a,*,1], Minju Oh [a,1], Ashraf Hossain [b,1], Keun Young Lee [c], Dayoung Yoo [b], Yangdo Kim [d], Sang-Woo Kim [c,e], Dongyun Lee [b,f,**]

[a] Department of Cogno-Mechatronics Engineering, Pusan National University, Busan 46241, Republic of Korea
[b] Department of Nano Fusion Technology, Pusan National University, Busan 46241, Republic of Korea
[c] School of Advanced Materials Science and Engineering, Sungkyunkwan University (SKKU), Suwon 16419, Republic of Korea
[d] School of Materials Science and Engineering, Pusan National University, Busan 46241, Republic of Korea
[e] SKKU Advanced Institute of Nanotechnology (SAINT), Center for Human Interface Nanotechnology (HINT), Sungkyunkwan University (SKKU), Suwon 16419, Republic of Korea
[f] Department of Nanoenergy Engineering, Pusan National University, Busan 46241, Republic of Korea

ARTICLE INFO

Article history:
Received 30 November 2016
Accepted 6 February 2017

Keywords:
Nanostructured materials
Zinc oxide
Titanium oxide
Buckling
Fracture

ABSTRACT

We calculated the mechanical properties of a ZnO nanorod within forest-like samples. According to the results for ZnO nanorods, we extended the calculation method to determine the mechanical properties of a TiO_2 nanotube (TN) extracted from a forest densely grown by anodization on a Ti substrate. The Euler model was adopted, and critical-load measurements were performed during vertical-compression experiments involving nanoindentation. We measured the elastic moduli of a single ZnO nanorod and a single TN as ~190 and ~27 GPa, respectively. Thus, we suggested a method for determining the mechaical properties of individual entities in one-dimensional materials grown in bundles.

In recent years, one-dimensional (1D) nanomaterials such as nanowires, nanotubes, and nanorods have attracted considerable interest for optical and chemical sensors, photocatalysts, and photoanodes in solar cells owing to their unique electrical properties [1–4]. From the viewpoint of the fabrication of electrical devices, the mechanical and functional properties of 1D nanomaterials should also be considered, because the reliability of devices is important. Furthermore, knowledge of the mechanical properties of individual 1D nanomaterials is a critical for applications in the field of nanomaterials. However, the agglomeration of 1D nanomaterials due to their high specific surface area and densely grown rods/wires on substrates has made it difficult to clarify the mechanical behavior of individual 1D nanostructures. We studied vertically grown ZnO nanorods and TiO_2 nanotubes (TNs) that were formed on GaN and Ti substrates, respectively. These nanostructured materials have been used for many electrical and optoelectronic devices [5,6].

Chen et al. reported [7] that the Young's modulus of ZnO nanowires was highly size-dependent and dramatically increased to 220 GPa as the diameter of the ZnO nanowires decreased to less than 120 nm [8]. In other studies, many different Young's moduli of ZnO were reported, depending on the size, fabrication methods, and measuring techniques [9,10]. In typical nanotube arrays, because the mechanical properties are determined by the constituent nanoelements, novel approaches are required to evaluate the strength of these discrete structures. For anodized nanoporous structures such as TNs, the modulus and hardness have been evaluated by a few research groups [11–13] using continuum mechanics [1,2,14]. Thus far, the mechanical properties of individual TNs have not been reported.

In previous studies, the mechanical properties of individual ZnO nanostructures were measured by complicated processes using microelectromechanical-systems [15,16] or *in situ* transmission electron microscopy [17,18], which are not only time-consuming and expensive but also difficult to perform. To resolve these issues, we carefully controlled the growth process to produce sparsely grown ZnO nanorods and then measured their mechanical properties. Using these data, we calculated the mechanical properties of a single ZnO nanorod within the forest-like samples. On the basis of the ZnO-nanorod example, we extended this methodology to determine the mechanical properties of an individual TN.

ZnO nanorods were grown on a 2-μm-thick GaN thin film by a wet chemical growth method using a zinc-nitrate solution. The density of the grown ZnO nanorods was controlled by seed layers, which are

* Corresponding author.
** Correspondence to: D. Lee, Department of Nano Fusion Technology, Pusan National University, Busan 46241, Republic of Korea.
E-mail addresses: siz0323@naver.com (J. Park), dlee@pusan.ac.kr (D. Lee).
[1] These authors contributed equally to this work.

http://dx.doi.org/10.1016/j.scriptamat.2017.02.011
1359-6462/

explained in detail in a previous report [19]. TNs were fabricated by the electrochemical anodization of a titanium foil. The detailed procedures for the fabrication of TNs are presented in a previous report [20]. To analyze the crystal structures of the ZnO nanorods and TNs, their X-ray diffraction patterns (Empyrean, PANalytical) were observed. The ZnO nanorods were preferentially grown along the c-axis direction [002], and the as-prepared TNs had an amorphous structure. The surface morphology of the samples and the size distribution of the nanorods and nanotubes were characterized before and after nanoindentation tests using a field-emission scanning electron microscope (FE-SEM SUPRA25, Zeiss and FE-SEM S-4700, Hitachi). Fig. 1 shows the scanning electron microscopy (SEM) images of the ZnO nanorods and TNs. Sparsely and densely grown ZnO nanorods are shown in Fig. 1(a) and (b), respectively. As shown in Fig. 1(a), the spaces between the nanorods were approximately 1–3 μm, which was large enough to allow the indentation of individual ZnO nanorods with a flat punch tip for the measurement of their mechanical properties. The diameter and height of the nanorods were approximately 500–850 nm and 3.5–4.5 μm, respectively. The diameter and height of the ZnO-nanorod bundle, which is shown in Fig. 1(b), were 150–450 and 1.8–2 μm, respectively, and the space between nanorods was ~300 nm. Using the flat punch tip, dozens of rods were simultaneously indented. Fig. 1(c) and (d) shows plane-view and side-view SEM micrographs of the TNs grown on the substrate at 50 V for up to 6 h. The average inner diameter (D_i) of the 6-h-grown TNs was ~112 nm, and the total diameter (D_e) was ~150 nm. The lengths of the 6-h-grown TNs were ~20 μm.

The mechanical properties of the ZnO nanorods and TNs were investigated using a nanoindentation system (Nanoindenter G200, Agilent Tech.). GaN and Ti metal sheets grown on 1D materials were glued onto a holder, and then an indentation test was performed with a flat diamond tip ($\phi = 2.5$ μm, Synton-MDP). Different stress states were applied to the contact region of the tip by using the flat punch shape indenter; thus, the inherent strength of the nanotubes was evaluated regardless of the loading conditions.

The indentation test was implemented with a constant strain rate of 0.05 s^{-1}, and the depth was varied from 500 to 1000 nm in order to gather complete information from the initial deformation to the final failure of the rods and tubes. Fig. 2 shows SEM images of a single ZnO nanorod and a bundle of ZnO nanorods after the indentation test (Fig. 2(a) and (b), respectively), as well as the indentation procedure for a single rod (Fig. 2(c)) and simulation data (Fig. 2(d)). Fig. 2(a) shows a representative image of the flat top tip on forest-like ZnO nanorods after the indentation experiment. With this type of failure, it is difficult to understand the mechanical properties of individual rods. We grew scanty ZnO nanorods and then indented them with the flat top tip. The spaces between the ZnO nanorods were wide enough for a single rod to be pushed through. An indented single ZnO nanorod is shown in Fig. 2(b). We presume that the ZnO nanorods broke near the interface between the GaN substrate and the nanorod. This was a commonly observed phenomenon during the study (refer to the enlarged inset in Fig. 2(b)). The reaction of the ZnO nanorod during indentation is schematically illustrated in Fig. 2(c). The ZnO nanorods were bent when the load applied to the rods reached the critical value, subsequently breaking near the interface between the GaN substrate and the nanorod. We used a computer simulation tool (COMSOL Multiphysics 4.2) to define the stress distribution in the ZnO nanorods under a load. As shown in Fig. 2(d), the stress applied to the rod was distributed from top to bottom and was highly concentrated at the edge of the bottom part, which may have caused the interfacial failure of the ZnO nanorods.

These phenomena are also observed in the load–displacement (L–D) curves shown in Fig. 3(a). A large displacement occurred when the segment was held during the indentation procedure, which is generally done for the stabilization of materials to deformation. In this procedure, the holding time was 10 s. Somehow, during the increase of the displacement, the load applied to the rods slightly decreased. Apparently, this was caused by the slip after the interfacial collapse of ZnO nanorods between the rods and substrate. Fig. 3(b) and (c) shows zoomed-in areas of the L–D curves from the initial loading to the sudden break, which is indicated by the dotted circle in Fig. 3(a). In Fig. 3(b) and (c), a few pop-ins are observed from 0 to 150 nm under displacement. Among them, it is reasonable to consider the first biggest increment in the displacement as the significant point for the critical load ($\boldsymbol{P_{cr}}$) of the nanorods, which can be used to evaluate the mechanical properties of the nanorods. Presumably, the sudden increase in the curve displacement around 60–80 nm were due to the initial buckling of the rods. This is reported in the literature as the “critical stable” zone II [21–23]. The

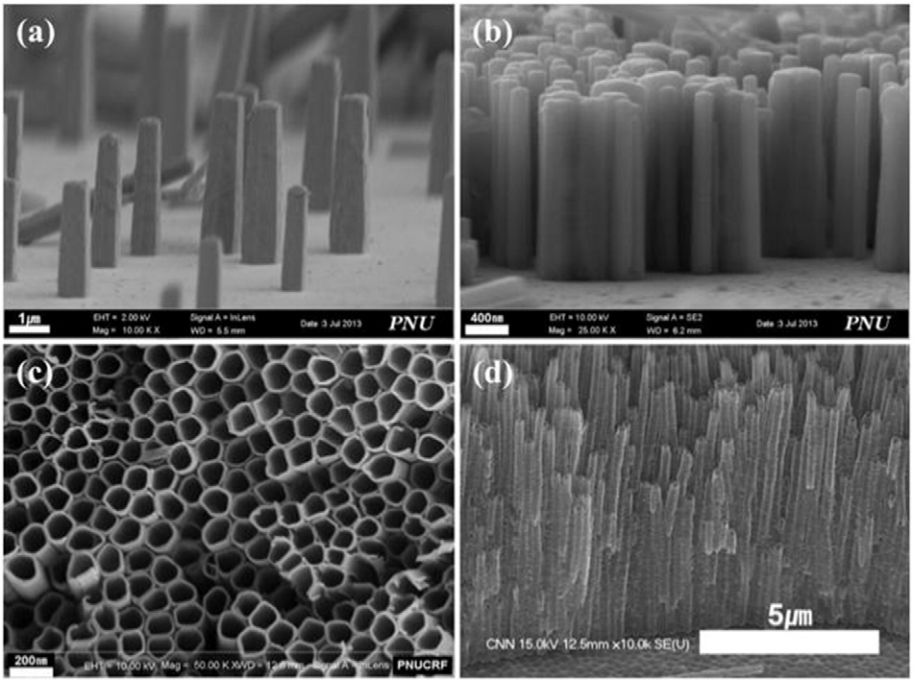

Fig. 1. SEM images of ZnO nanorods (a, b) and TNs (c, d): (a) ZnO nanorods grown sparsely with special care by a wet chemical growth method; (b) densely grown ZnO bundle; (c) top view of anodized TNs; (d) side view of (c) showing uneven heights.

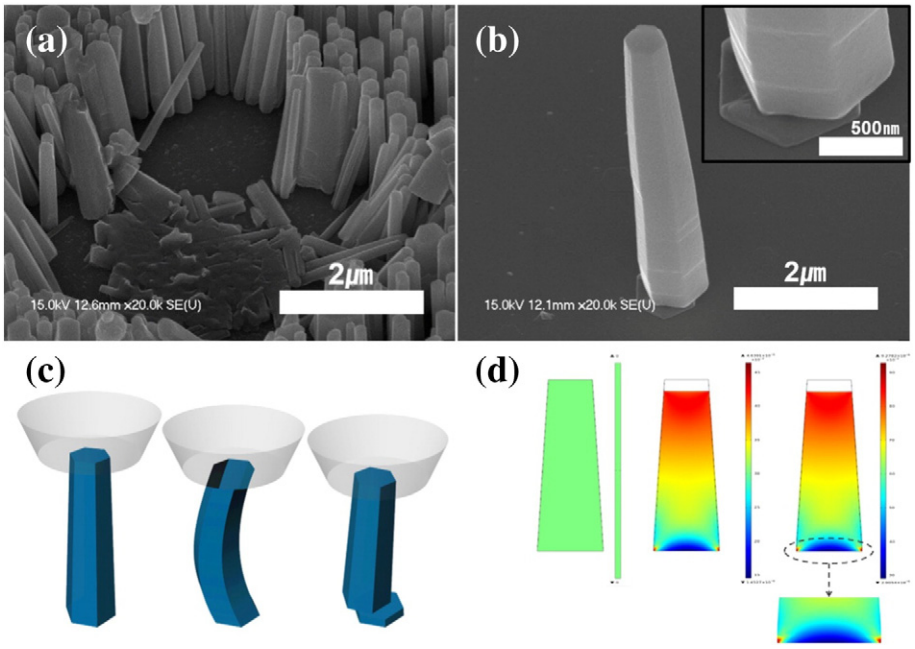

Fig. 2. SEM images of (a) a loaded forest of ZnO nanorods and (c) a single loaded ZnO nanorod; (c) illustration of the indentation procedure for a single ZnO nanorod; (d) stress concentration distribution in ZnO nanorods.

behavior of an ideal column and/or rod compressed by an axial load $\boldsymbol{P}$ can be summarized as follows: (1) if $\boldsymbol{P} < \boldsymbol{P_{cr}}$, the column is under a stable equilibrium in the straight position; (2) if $\boldsymbol{P} = \boldsymbol{P_{cr}}$, the column is under a neutral equilibrium in either the straight position or a slightly bent position; (3) if $\boldsymbol{P} > \boldsymbol{P_{cr}}$, the column is under an unstable equilibrium in the straight position and buckles under the slightest disturbance.

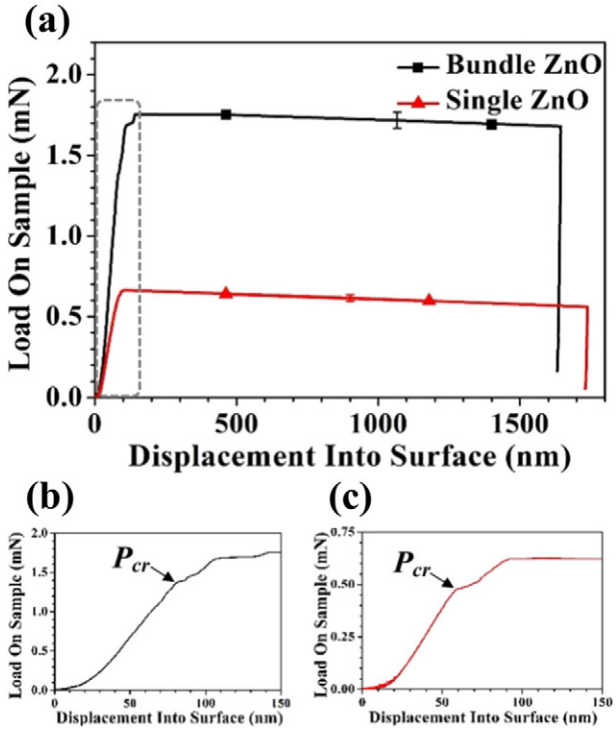

Fig. 3. L–D curves for the indentation of a bundle of ZnO nanorods and a single ZnO nanorod, along with simulation results. (a) Representative L–D curves of a bundle of ZnO nanorods and a single ZnO nanorod; magnified curve of (b) a bundle of nanorods and (c) a single nanorod indicated by the dotted line in (a).

The critical loads of a single nanorod and a bundle of ZnO nanorods were approximately 0.47 ± 0.01 and 1.3 ± 0.02 mN, respectively. Several pop-in events in the bundle ZnO nanorod sample (Fig. 3(b)) were observed after the critical load was applied, possibly owing to the buckling of several nanorods with different heights during the densification [21]. Two models are available for calculating the modulus using the critical load. To determine which is suitable, $\left(\frac{l}{k}\right)_{p}$, and $\left(\frac{l}{k}\right)_{actual}$, were compared. Because $\left(\frac{l}{k}\right)_{actual}$, was bigger than $\left(\frac{l}{k}\right)_{p}$, the Euler model was used. The Euler model may be the correct choice to understand how ZnO nanorods mechanically behave under typical compressive loads with relatively high slenderness ratios [23]. The general form of the Euler equation for a straight column under uniaxial compression is

$$p_{cr} = \frac{C\pi^2 EI}{l^2}, \tag{1}$$

where C is a constant that depends on the column end conditions, E is the modulus of elasticity, I is the momentum of inertia, and l is the length of the column. In this study, the end conditions of column were "fixed-free," so the theoretical value of the constant C is 0.25, and the momentum of inertia corresponds to $I = Ak^2$, where k is the radius of gyration of the column. Therefore, Eq. (1) can be rewritten as follows:

$$\frac{p_{cr}}{A} = \frac{C\pi^2 E}{\left(\frac{l}{k}\right)^2}, \tag{2}$$

where l/k is the slenderness ratio, $k = \left(\frac{I}{A}\right)^{\frac{1}{2}}$, $I = \frac{\pi D^2}{64}$ is the moment of inertia of the nanorod, D is the diameter of the nanorod, $A = \frac{\pi D^2}{4}$ is the area of the nanorod, and $\frac{p_{cr}}{A}$ is the unit load. Therefore, Eq. (2) can be rewritten as

$$E = \frac{4l^2 p_{cr}}{C\pi^3 D^4} \tag{3}$$

The average critical load, diameter, height, and modulus of the ZnO nanorods were calculated using the Euler model. The modulus of an individual ZnO nanorod was ~184.62 ± 5.56 GPa. The modulus of a ZnO

nanorod in a bundle was calculated by dividing the number of ZnO nanorods indented underneath the flat top tip as ~191.56 ± 3.37 GPa. In the literature [7], there are reports on the significant effect of the size of ZnO nanorods on the modulus below a diameter of 120 nm, whereas the size effect for ZnO nanorods with a diameter larger than 120 nm is diminished in comparison. Because the diameters of the ZnO nanorods investigated in this study were larger than 120 nm, it is surprising that the obtained elastic moduli were far higher than that of bulk: ~140 GPa. As reported, the moduli of a single nanorod and a and bundle of ZnO nanorods were ~190 GPa, which is higher than the values reported in the literature [7]. The difference in modulus might have been due to the experimental technique. During the compression test along the axial direction, the influence of the defects in the nanorods on their mechanical properties can be notably reduced. The important aspect of this work is that the mechanical properties of an individual nanorod within densely grown nanorods can be easily determined.

Plane-view SEM micrographs of the TNs after the nanoindentation test are shown in Fig. 4(a) and (b), which correspond to indentation depths of 1000 and 500 nm, respectively. Owing to the uneven length of the TNs and the 70° tip angle, the indented area was far larger than the flat top tip area with increasing indentation depth, which is indented by white circles in Fig. 4(a) and (b). A standard micrographic technique was employed to calculate how many TNs were indented. More than five samples were each tested ten times with a prescribed testing schedule, and the results were reproducible. Fig. 4(c) shows the L–D curves of specimens anodized for 6 h at indentation depths of 500 and 1000 nm from the end of the TNs. These curves exhibit average values after more than 10 indentation tests. The inset in Fig. 4(c) shows enlarged L–D curves of the initial loading part for determining the critical load $\boldsymbol{P_{cr}}$, which is indicated by arrows. As shown in this enlarged curve, several pop-in-like behaviors were observed during the indentation. The first significant pop-in was ascribed to the critical load ($\boldsymbol{P_{cr}}$). The surface of the TNs arrays was rough owing to the different height of the tubes; thus, the first pop-in in the graph corresponds to the critical load. The average critical loads of the TNs after 6 h at indentation depths of 500 and 1000 nm were approximately 10.07 and 11.91 μN, respectively. The 1000-nm-depth indentation data were used to identify the mechanical properties of the TNs. Subsequently, we calculated the modulus of a single TN by using the same method as the one employed for ZnO nanorods. Because TNs are hollow structures, the moment of inertia is determined as follows:

$$I = \frac{\pi\left(D_e{}^4 - D_i{}^4\right)}{4}, \tag{4}$$

where D_e and D_i are the external and inner diameter, respectively, of the TNs. Therefore, Eq. (3) can be rewritten as

$$E = \frac{4l^2 p_{cr}}{0.25\pi^3\left(D_e{}^4 - D_i{}^4\right)} \tag{5}$$

According to Eq. (4), the calculated modulus of the TNs after 6 h is ~27 GPa. In previous studies, a wide range of elastic moduli of TNs have been reported, e.g., within the range of 2.2–44 GPa [1,2,22]. We found that the elastic modulus of the TNs was 27 GPa, which is similar to the 10-nm value of thin-walled TNs reported by Shokuhfar et al. [1]. The authors reported that the elastic modulus of a single TN with external and internal nominal diameters of ~75 and ~65 nm, respectively, was ~23 GPa. In addition, they reported a far higher elastic modulus—44 GPa—of TNs with a thick wall of 30 nm. In this study, the dimensions of the TNs were slightly larger than those of the reported TNs, and the external and internal nominal diameters were ~150 and ~112 nm, respectively. However, TNs twice as long were used for measuring the elastic modulus, presumably yielding a lower elastic modulus than the thick-walled samples. The potential presence of structural defects in the TNs increases with the dimensions. It can be assumed that the ratio between the wall thickness and the length of the TNs is closely related to the elastic modulus of nanotubes.

Critical-load measurements during vertical-compression experiments involving nanoindentation were used to calculate the mechanical properties of the ZnO nanorods and TNs. In this study, we focused on the calculation of the mechanical properties of a single ZnO nanorod within forest-like samples. According to the results for ZnO nanorods, we extended our calculation method to define the mechanical properties of an individual TN extracted from a forest densely grown by anodization of a Ti substrate. The Euler model was adopted, and then the elastic moduli of a single ZnO nanorod and a single TNs were successfully measured as ~190 and ~27 GPa, respectively. The method proposed in this study can be used to determine the mechanical properties of an entity in any type of 1D material grown in a bundle.

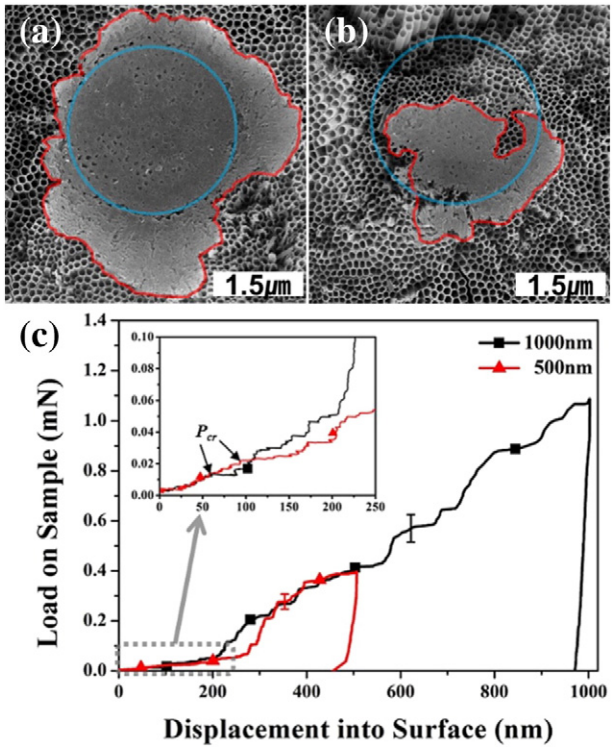

Fig. 4. SEM images of 6-h-grown TNs indented at loading depths of (a) 1000 and (b) 500 nm; (c) representative L–D curves for the indentation of 6-h-grown TNs at depths of 500 and 1000 nm depth. The inset shows enlarged L–D curves with the indication of the critical loads.

Acknowledgements

This research was co-supported by 1) the National Research Foundation of Korea (NRF) grant funded by the Korea government (MSIP) (No. 2015R1A2A2A01002795); 2) a National Research Foundation of Korea (NRF) grant funded by the Korea government (MSIP) (NRF-2014R1A2A2A01007428); 3) the Civil & Military Technology Cooperation Program, through the National Research Foundation of Korea (NRF), funded by the Ministry of Science, ICT & Future Planning (No. 2013M3C1A9055407).

References

[1] T. Shokuhfar, G.K. Arumugam, P.A. Heiden, R.S. Yassar, C. Friedrich, ACS Nano 3 (2009) 3098.
[2] G.A. Crawford, N. Chawla, K. Das, S. Bose, A. Bandyopadhyay, Acta Biomater. 3 (2007) 359.
[3] H. Hirakata, K. Ito, A. Yonezu, H. Tsuchiya, S. Fujimoto, K. Minoshima, Acta Mater. 58 (2010) 4956.

[4] J.M. Macak, H. Tsuchiya, A. Ghicov, K. Yasuda, R. Hahn, S. Bauer, P. Schmuki, Curr. Opin. Solid State Mater. Sci. 11 (2007) 3.
[5] S. Oh, K. Shin, S. Kim, S. Lee, H. Yu, S. Cho, K. Kim, J. Nanosci. Nanotechnol. 13 (2013) 3696.
[6] M.A. Hossain, J. Park, J.Y. Ahn, C. Park, Y. Kim, S.H. Kim, D. Lee, Electrochim. Acta 173 (2015) 665.
[7] C.Q. Chen, Y. Shi, Y.S. Zhang, J. Zhu, Y.J. Yan, Phys. Rev. Lett. 96 (2006) 075505.
[8] I. Kobiakov, Solid State Commun. 35 (1980) 305.
[9] S.J. Young, L.W. Ji, S.J. Chang, T.H. Fang, T.J. Hsueh, Physica E 39 (2007) 240.
[10] F. Xu, Q. Qin, A. Mishra, Y. Gu, Y. Zhu, Nano Res. 3 (2010) 271.
[11] S. Ko, D. Lee, S. Jee, H. Park, K. Lee, W. Hwang, Thin Solid Films 515 (2006) 1932.
[12] Z. Xia, L. Riester, B. Sheldon, W. Curtin, J. Liang, A. Yin, J. Xu, Rev. Adv. Mater. Sci. 6 (2004) 131.
[13] T. Fang, T. Wang, C. Liu, L. Ji, S. Kang, Nanoscale Res. Lett. 2 (2007) 410.
[14] X. Tang, D. Li, J. Phys. Chem. C 113 (2009) 7107.
[15] A.V. Desai, M.A. Haque, Sensors Actuators A 134 (2007) 169.
[16] H. Ni, X. Li, Nanotechnology 17 (2006) 3591.
[17] X. Bai, P. Gao, Z.L. Wang, E. Wang, Appl. Phys. Lett. 82 (2003) 4806.
[18] Y. Huang, X. Bai, Y. Zhang, J. Phys. Condens. Matter 18 (2006) L179.
[19] S. Lee, Y. Kim, M. Yi, J. Choi, S. Kim, J. Phys. Chem. C 113 (2009) 8954.
[20] M.A. Hossain, J. Park, J.Y. Ahn, C. Park, Y. Kim, S.H. Kim, D. Lee, Electrochim. Acta 173 (2015) 665.
[21] M. Riaz, A. Fulati, Q. Zhao, O. Nur, M. Willander, P. Klason, Nanotechnology 19 (2008) 415708.
[22] S.P. Timoshenko, J.M. Gere, Theory of Elastic Stability, second ed. Dover Publications, New York, 2009.
[23] R.G. Budynas, J.K. Nisbett, Shigley's Mechanical Engineering Design, ninth ed. McGraw-Hill, New York, 2011.